Optical Materials 163 (2025) 116901

Contents lists available at ScienceDirect

Optical Materials

journal homepage: www.elsevier.com/locate/optmat

Research article

Thermal noise reduction in ion-beam sputtered HfO_2:Ta_2O_5 thin films via high-temperature treatment

Valeria Milotti [a,*], Giulio Favaro [a,1], Massimo Granata [b], Danièle Forest [b], Christophe Michel [b], Julien Teillon [b], Nicole Busdon [a], Marco Bazzan [a], Hanna Skliarova [a], Giacomo Ciani [a,2], Carlo Scian [a], Livia Conti [c], Shima Samandari [d], Valentina Venturino [d], Michele Magnozzi [d], Maurizio Canepa [d], Nicholas Demos [e], Slawomir Gras [e], Matthew Evans [e], Valérie Martinez [f], Gianpietro Cagnoli [f], Nikita S. Shcheblanov [g,h], Anaël Lemaître [h]

[a] Università di Padova, Dipartimento di Fisica e Astronomia, via Marzolo, 8, Padova, 35131, Italy
[b] Laboratoire des Matériaux Avancés – IP2I, CNRS, Université Claude Bernard Lyon 1, Villeurbanne, 69100, France
[c] INFN Padova, via Marzolo, 8, Padova, 35131, Italy
[d] OptMatLab, Dipartimento di Fisica, Università di Genova, Genova, Italy
[e] Massachusetts Institute of Technology, NW22-295, 185 Albany Street, Cambridge, 02139, MA, USA
[f] Institut Lumière Matière, UMR5306 CNRS Université Claude Bernard Lyon 1, Villeurbanne, France
[g] MSME, Univ Gustave Eiffel, CNRS, Univ Paris Est Créteil, UMR 8208, Marne-la-Vallée, 77454, France
[h] Navier, Ecole des Ponts, Univ Gustave Eiffel, CNRS, Marne-la-Vallée, France

ARTICLE INFO

Keywords:
Coating thermal noise
HfO_2:Ta_2O_5
Thin films
Crystallization
Optical characterization

ABSTRACT

Reducing coating thermal noise (CTN) in mirrors for gravitational wave (GW) interferometers is pivotal to improving sensitivity in the mid-frequency range. Current mirror coatings are heat-treated (annealed) after deposition in order to partially relax their microstructure and to improve their optical and mechanical properties. The maximum annealing temperature is an important parameter in this respect as a higher thermal energy allows the system to relax to more stable configurations, which is often beneficial for the thermal noise performances of the coatings. However, the useful temperature range is limited by the stability of the amorphous microstructure, since excessive heating eventually leads to the formation of crystalline grains which are detrimental from both the mechanical and optical viewpoints. In this work, inspired by the possibility to improve glass stability in alloys by a careful choice of mixing ratios, we studied ion-beam co-sputtered amorphous HfO_2:Ta_2O_5 thin films with different HfO_2 concentrations, so as to identify conditions that would lead to a higher glass stability in order to explore the effects of a thermal annealing over an extended temperature range. We then deposited a multilayer mirror, alternating layers of HfO_2:Ta_2O_5 with composition providing the highest crystallization temperature and SiO_2 layers. The thermal Brownian noise of the mirror coating was found to decrease with increasing heat-treatment temperatures, reaching losses comparable to the Ti-doped Ta_2O_5 coatings of Advanced LIGO when heated at the highest possible temperature. Our results demonstrate the critical importance of optimizing the film composition and annealing procedure in order to improve the coating performances and the sensitivity for the next generation of GW detectors.

1. Introduction

Current second-generation and planned third-generation gravitational-wave (GW) detectors are Michelson interferometers, whose arms are kilometers-long Fabry–Perot cavities [1]. The test masses used in GW interferometers consist of super-polished, highly transparent substrates weighing tens of kg [2,3], whose surface is coated with highly reflective (HR) stacks of alternating low and high refractive index (LI and HI, respectively) materials, designed to work as

* Corresponding author.
E-mail address: valeria.milotti@unipd.it (V. Milotti).
[1] Present affiliation: Consiglio Nazionale delle Ricerche - Istituto di Fotonica e Nanotecnologie (CNR-IFN), via Trasea, 7, Padova, Italy
[2] Present affiliation: Università di Trento, Dipartimento di Fisica, via Sommarive 14, 38123 Povo (TN), Italy

https://doi.org/10.1016/j.optmat.2025.116901
Received 27 November 2024; Received in revised form 6 February 2025; Accepted 4 March 2025
Available online 22 March 2025

Bragg reflectors at the detector's laser wavelength [4–6]. Present GW interferometers, namely LIGO in the USA, Virgo in Italy, and KAGRA in Japan, employ amorphous layers of SiO_2 as the LI material and Ti-doped Ta_2O_5 as the HI material [4,7–9], which are deposited by Ion-Beam Sputtering (IBS). Since future third-generation detectors such as Einstein Telescope [10] and Cosmic Explorer [11] will likely use similar technologies, the identification of amorphous materials with improved properties for future coatings is a matter of intense research efforts [12–14].

A major challenge in upgrading second-generation and developing third-generation GW detectors is increasing their sensitivity. Achieving this goal requires, in particular, reducing coating thermal noise (CTN), which is the dominant contributor to the overall noise budget in the relevant frequency range (around 100 Hz) in room temperature interferometers (which includes LIGO [15], Virgo [3], and the high-frequency detector of ET [16]).

Thermal noise is a common feature of amorphous solids and results from the fact that their disordered microstructures tend to accommodate local multistable configurations that may undergo thermally-activated transitions over broadly distributed activation barriers [17–22]. Although the precise nature of these transitions remains a matter of debate, they are expected to be all the more prevalent if a glass is poorly relaxed, which explains their preponderance in IBS-deposited coatings. A main advantage of the IBS technique is that it allows film growth close to room temperature, i.e. well below bond energies for oxides, which stifles atomic diffusion during growth. This guarantees a very high degree of material homogeneity and isotropy in the as-deposited material, which is an essential precondition to achieving the required outstanding optical properties. As a result, however, the as-deposited films are strongly out-of-equilibrium, in the sense that, in sharp contrast with melt-quenched glasses, they have not experienced any equilibrium liquid state. This favors the existence of a high density of multistable atomic packings. In IBS-deposited silica (the usual low-index layers) the corresponding barriers tend to be quite small, hence giving rise to a harmless high-frequency noise contribution in room-temperature interferometers. On the contrary, high-index IBS-deposited layers tend to form multistable regions that are thermally active in the observation frequency range at room temperature, and are the primary source of CTN in the current oxide coatings.

CTN can be reduced by improving the degree of relaxation of the material constituting these high-index layers, which can be performed via a post-deposition annealing. Indeed, this has become a standard treatment for IBS-deposited mirror coatings. For example, the stacks of Ti-doped Ta_2O_5 and SiO_2 layers in use in current GW detectors are annealed at 500 °C for 10h [4].

Ideally, one would want to anneal these stacks close to and below the glass transition temperature of the high-index oxide, since these conditions favor the formation of the most stable glasses for a given material [23–28]. But high-temperature annealing may eventually introduce defects in the coating layers, primarily due to the onset of crystallization [29], thus leading to a degradation of their optical and mechanical properties.[3] Hence, the possibility to achieve a significant relaxation of a glass and a measurable reduction of thermal noise via annealing depend on its ability to relax towards supercooled liquid equilibrium states without crystallizing, a property known as *thermal stability* [30–32].

It appears therefore promising to explore the impact of a high temperature annealing on the CTN, which requires to identify suitable coating materials with improved thermal stability .

The thermal stability of glasses and a closely related property, their glass forming ability or GFA (i.e. their stability against crystallization during a thermal quench) [30,33], have received considerable attention in studies of metallic alloys due to the tremendous difficulties in limiting crystallization for these systems. In this context, it has been shown that thermal stability and GFA can be strongly enhanced by identifying mixtures (alloys) of precise composition [30,34] that hinder the crystallization .

In this work, we test this strategy by exploring the HfO_2/Ta_2O_5 system, as both these two oxides have high refractive indices, low optical absorption [35,36], and produce ceramics with high crystallization temperatures [37]. We deposited mixed HfO_2:Ta_2O_5 (hafnia-tantala) coating samples with different ratios of the two oxides searching for the composition ensuring the highest thermal stability. For each ratio, samples were annealed at temperatures between 500 °C and 900 °C, maintaining the target temperature for 10 h to allow for easier comparison with the standard treatment. Annealed samples were then analyzed *ex-situ* by X-ray diffraction to detect the presence of a crystallized fraction. The composition displaying the highest thermal stability has then been used to fabricate a SiO_2/HfO_2:Ta_2O_5 high-reflectivity multilayer and annealed at high temperature to allow for a direct characterization of the coating thermal noise.

2. Experimental methods

2.1. Deposition and treatment of samples

2.1.1. Coating deposition

The thin-film samples used in this work were deposited in a large custom-developed Ion Beam Sputtering (IBS) facility [38] at the Laboratoire des Matériaux Avancés (LMA), the same facility used to coat the mirrors of present GW interferometers [4]. Argon ions accelerated to ∼ 1 keV were used as sputtering particles. Prior to deposition, the base pressure inside the facility vacuum chamber was below 10^{-5} mbar; during deposition, the working pressure was of the order of 10^{-4} mbar and composed mainly of argon and oxygen.

Samples were ∼ 400 nm to ∼ 600 nm thick and grown on several different substrates made of fused silica (that is, amorphous SiO_2; 25.4 mm diameter, 6 mm thick) and (100) p-doped silicon (76.2 mm diameter, 0.5 mm thick) at the same time, with the purpose of performing different specific characterizations afterwards. During deposition, substrates were heated up to a temperature between 100 and 150 °.

The HfO_2 concentration found to yield the highest crystallization temperature was then used to design and deposit a multi-layer HR sample. Such HR sample is a Bragg reflector composed of 41 layers of HfO_2:Ta_2O_5 (HI) and SiO_2 (LI), deposited on a Si substrate. Its total thickness is 6.56 μm, with 2.65 μm of HfO_2:Ta_2O_5 and 3.91 μm of SiO_2.

2.1.2. Sample treatment

Thermal treatments were carried out in a Carbolite CTF 12/75/700 oven in ambient atmosphere. The current standard treatment for coatings is a post-deposition annealing at 500 °C for 10 h. Different as-deposited samples from each batch (i.e. for each composition) were annealed at different temperatures in order to find the crystallization threshold. We used temperatures spaced by 100 °C between 500 °C and 900 °C. Each as-deposited sample was maintained at the target temperature for 10 h, as in the standard treatment, with a ramp of 100 °C/hour in order to minimize stresses in the coatings and distortions caused by heating. With this process, we produced five different samples annealed at different temperatures for each HfO_2:Ta_2O_5 composition. For the most promising samples, once the approximate crystallization threshold was established, we repeated the annealing investigation around the crystallization temperature in steps of 50 °C for better accuracy.

[3] In principle, partial crystallization (with e.g. the formation of small nuclei) could be used to reduce mechanical loss, but doing so requires a high degree of control of crystal growth, which also requires the deposited material having a high thermal stability.

Table 1
Chemical composition, HfO_2 molar concentration and estimated crystallization temperature after 10 h of annealing of as-deposited samples. The errors bars refer to the statistical errors associated with fitting of the luminescence spectra.

Sample	Hf (At%)	O (At%)	Ta (At%)	Ar (At%)	HfO_2 (mol%)	Cryst. Temp. (°C)
A	27.3 ± 0.4	66 ± 2	2.7 ± 0.5	4.4 ± 0.3	95.3 ± 0.8	Room Temp.
B	26.4 ± 0.4	65 ± 2	3.2 ± 0.4	5.2 ± 0.3	94.3 ± 0.7	Room Temp.
C	24.8 ± 0.4	66 ± 2	4.2 ± 0.4	5.3 ± 0.3	92.2 ± 0.7	650 ± 50
D	22.1 ± 0.4	66 ± 4	6.5 ± 0.2	5.2 ± 0.3	87.2 ± 0.4	750 ± 50
E	20.7 ± 0.3	66 ± 2	7.8 ± 0.4	5.2 ± 0.3	84.1 ± 0.7	750 ± 50
F	18.7 ± 0.3	68 ± 2	9.1 ± 0.4	4.2 ± 0.3	80.4 ± 0.7	750 ± 50
G	16.7 ± 0.3	67 ± 2	11.5 ± 0.4	4.9 ± 0.3	74.4 ± 0.7	850 ± 50
H	12.2 ± 0.3	69 ± 2	14.7 ± 0.4	4.1 ± 0.3	62.4 ± 0.9	850 ± 50
I	11.7 ± 0.1	68 ± 1	16.3 ± 0.1	3.8 ± 0.1	58.9 ± 0.2	825 ± 25
J	6.3 ± 0.5	70 ± 4	19.3 ± 0.6	4.3 ± 0.6	39.5 ± 2.0	850 ± 50
K	3.97 ± 0.1	67 ± 1	25.3 ± 0.1	3.3 ± 0.1	23.9 ± 0.4	775 ± 25

2.2. Characterization techniques

2.2.1. Energy-Dispersive X-ray (EDX) spectroscopy

Energy-Dispersive X-ray (EDX) Spectroscopy was performed by analyzing *ex-situ* sample X-ray fluorescence on a Zeiss Sigma HD field emission electron microscope.

The technique provides an estimate of the atomic concentration At_x of each element x, shown in Table 1. Beyond statistical errors associated with sensitivity limits (which are reported in Table 1) EDX measurements are affected by a systematic error resulting from the fact that the contribution of a given atom type to the fluorescence may deviate from its theoretical estimate (mainly proportional to the atomic mass) as a result of various effects, which can be modeled as a correction factor [2]. However, for heavy atoms of close-by masses, which is the case of Hf and Ta, the correction factors are almost equal, so that these systematic errors can be eliminated by considering their molar ratio. For this reason, we characterize the film composition by the molar ratio of HfO_2 with respect to the total oxide concentration, namely:

$$HfO_2(\text{mol\%}) = 100 \cdot \frac{2At_{(Hf)}}{(2At_{(Hf)} + At_{(Ta)})}$$

which we can consider to be essentially free of any systematic error.

2.2.2. Grazing Incidence X-Ray Diffraction (GIXRD)

We performed *ex situ* Grazing Incidence X-ray Diffraction (GIXRD) measurements to identify phase changes in the coatings after annealing. We used a PANalytical MRD Diffractometer equipped with a Cu tube operated at 40 kV, 40 mA. A parabolic multilayer mirror and a slit were used to collimate and improve spectral purity of the radiation from the Cu K_α line. We used a Xe proportional counter as detector, which was equipped with a parallel plate collimator mounted in front of it, providing an angular acceptance in the scattering plane of about 0.1 degrees. A Soller slit was inserted in order to limit axial acceptance to 0.04 radians. A grazing incidence configuration was used to enhance the scattering signal from the thin film. The diffraction spectrum for all samples was measured by keeping the primary beam fixed at an incidence angle of 1° with respect to the sample surface and moving the detector goniometer (2θ-scan) with 2θ ranging from 15 ° to 100 °.

Plausible crystalline phases were found using the program QualX 2.0 [39,40] and the Crystallography Open Database [41–48].

2.2.3. Optical microscopy

Samples were inspected visually using a Keyence VHX-7000 digital microscope. In order to enhance crystal visibility, coaxial lighting was used together with a pair of polarizing filters placed in the optical path, following the procedure from [29].

2.2.4. Atomic Force Microscopy

Atomic Force Microscopy (AFM) was used to study the surface morphology of non-crystallized, partially crystallized and completely crystallized samples. Measurements were carried out in semicontact/tapping mode on a Nanosurf FlexAFM setup equipped with a PPP-NCHR cantilever with a force constant of 42 N/m and resonance frequency of approximately 330 kHz.

2.2.5. Micro-Raman spectroscopy

In order to determine the influence on vibrational properties of varying the HfO_2 content, we acquired Raman spectra with a Horiba XploRA Plus spectrometer, at exciting laser wavelengths of 532 nm. We used as-deposited samples on SiO_2 for the Raman characterization, as the background signal from a Si substrate would overwhelm the signal from the coatings.

2.2.6. Spectroscopic Ellipsometry (SE)

The optical characterization was performed using spectroscopic ellipsometry (SE). We analyzed the coatings in a broad spectral range from 190 to 2500 nm (0.5–6.5 eV) utilizing the Variable Angle Spectroscopic Ellipsometer (VASE) from J. A. Woollam Co., Inc.. A wide spectral range is necessary to determine the energy gap, which, for the materials considered in this work, lies in the UV range. At the same time, this range provides refractive index data relevant to GW detector mirrors, which currently operate at 1064 nm but may shift to longer wavelengths (1550 or 2000 nm) in the future. Ellipsometry determines two quantities conventionally named Ψ and Δ. Δ is the phase difference between the electric fields parallel and perpendicular to the plane of incidence, while Ψ is defined as:

$$\Psi = \text{atan}\left(\frac{|r_p|}{|r_s|}\right) \tag{1}$$

where r_p and r_s are the complex Fresnel coefficient of the sample. According to the previous definitions, Ψ and Δ are angles. To maximize the SE data accuracy, Ψ and Δ spectra were obtained at three angles of incidence (60 °, 65 °, and 70 °), in proximity to the samples' Brewster angle [49]. The refractive index n, thickness t and energy gap E_g of the samples were derived by fitting the acquired spectra with a Cody Lorentz optical model, using a strategy detailed in a previous publication [50]. Data analysis was performed with the J. A. Woollam software WVASE [51].

2.2.7. Coating thermal noise measurements

Coating thermal noise (CTN) measurements were conducted with a multi-mode technique [52,53] using a folded standing-wave Fabry–Perot cavity, where the folding mirror was the coating sample. Each of the co-resonating second-order orthogonal transverse modes, TEM02 and TEM20, acts as a cavity length sensor for a different region of the coating surface. Any noise common to both TEMs cancels out on the beat frequency between these modes, whereas noise from thermally induced vibrations in separate regions of the coating adds in quadrature. The beat frequency, around ~ 5 MHz, occurs as a result of astigmatism in the cavity end mirrors. This technique allows for the routine measurement of thermal noise spectra in the frequency band from ∼ 30 Hz to ∼ 3 kHz. The large sensitivity of this experimental setup also allows us to measure the cavity response to thermal load and thus estimate the optical absorption of the coating.

In early CTN measurements that used this technique [52,53], it was assumed that the cavity end mirrors contributed negligibly to the measured CTN. For the results presented here, however, we properly accounted for their contribution [54].

The multi-mode technique is currently the preferred method of the LIGO Collaboration for performing CTN measurements of HR coatings.

3. Experimental results

3.1. Thin film composition

The first step of our analysis was to determine the composition of the deposited thin films. We measured the chemical composition through EDX on all samples, both as-deposited and after annealing at 900 °C. In all samples the main detectable elements were Hf, Ta, O and Ar. Results are reported in the first four columns of Tables 1 and S.I. Sample compositions remained stable after annealing, while the Ar content either decreased significantly or vanished completely. This is consistent with previously reported Ar heat-stimulated outgassing from coatings during annealing [55]. Results were reproducible across different locations on the coating.

To more thoroughly assess sample homogeneity, we mapped EDX spectra over several small areas on as-deposited and crystallized samples from the K and I batches. This analysis confirmed that Hf and Ta are homogeneously distributed within the investigated areas at our instrument's resolution (see Figure S.1).

By repeating the measurements several times, we found that the relative statistical uncertainty in the measured composition of each element's percentage was $\leq$ 0.5 At%. In order to remove the unknown systematic error component from the data, as explained in Section 2.2.1, we calculated the HfO_2 molar percentage of each batch. The results of this analysis for each sample are shown in the fifth column of Tables 1 and S.I. This computation provided a reliable composition estimate, allowing us to compare samples with each other and with available literature.

3.2. Crystallization threshold and morphology

As-deposited samples for each coating mix were annealed at 600 °C, 700 °C, 800 °C and 900 °C. After annealing, samples were measured by *ex-situ* Grazing Incidence X-ray Diffraction (GIXRD) to detect the onset of diffraction peaks and thus identify the approximate crystallization temperature. Resulting GIXRD diffractograms are reported in Figure S.2. All samples that had been annealed at the highest investigated temperature, 900 °C, showed crystallization peaks, as shown in Fig. 1(a). The crystallization threshold was estimated as the halfway point between the highest annealing temperature not inducing crystallization and the lowest annealing temperature for which diffraction peaks were present. This analysis demonstrates that the crystallization temperature of our mixtures is highly sensitive to the HfO_2:Ta_2O_5 ratio, as shown in the data reported in the last column of Table 1, highlighting an alloying effect on the glass stability.

The samples with the highest HfO_2 concentration, A and B, showed small crystallization peaks as deposited (see Figures S.2(a,b)). For reference, pure Ta_2O_5 coatings crystallize at about 630 °C for the same annealing duration [29].

Samples with HfO_2 concentrations between 25% and 65% showed the highest crystallization temperature, exceeding 800 °C. Two of these compositions, batches I and K, underwent a more thorough investigation in order to precisely determine their crystallization temperature. As can be seen from Fig. 1(c), sample I starts showing diffraction peaks when annealed at 850 °C, thus we estimate the crystallization temperature for batch I to be between 800 °C and 850 °C. In contrast, diffraction peaks arise in the spectrum of sample K between 750 °C and 800 °C, at a slightly lower temperature than expected (see Figure S.3). As batch I was confirmed to have the highest crystallization temperature, we prioritized it for the more in-depth and time-consuming characterization techniques.

To further understand the crystallization processes, we analyzed the diffractograms of samples with different compositions annealed at 900 °C. By combining these diffractograms with the compositional data found in Section 3.1, we found that our results could be explained by the presence of three crystalline phases — monoclinic HfO_2, orthorhombic Ta_2O_5, and orthorhombic $Hf_6Ta_2O_{17}$ [57] – appearing in different ratios depending on the molar percentage of HfO_2. The phase mixes we used to model the experimental GIXRD diffractograms are reported in Fig. 1(b). A previous study by McCormack et al. on a similar system described the phase space of $Ta_2O_5-HfO_2$ mixed oxides as a function of molar HfO_2 concentration vs. annealing temperature [58]. By superimposing the crystalline phases found in our annealed samples to this graph, we notice that our data are in agreement with the expectation based on the phase diagram of $Ta_2O_5-HfO_2$ alloys. In particular, all mixes with HfO_2 concentration between 25% and 65%, for which we found the highest crystallization thresholds, produce Ta_2O_5 and $Hf_6Ta_2O_{17}$ crystalline phases.

We used optical microscopy to visually inspect as-deposited and annealed samples for all HfO_2:Ta_2O_5 mixes. We report results for sample I in Figs. 2(a–d). The as-deposited sample is optically homogeneous, without any relevant features, as expected from the absence of crystallization observed with GIXRD. High-temperature annealing, up to 800 °C, left the sample optically homogeneous, consistent with the absence of diffraction peaks in GIXRD diffractograms, except for the appearance of bubbles, which will be discussed later.

When the annealing temperature reached 850 °C and its GIXRD spectrum began to show diffraction peaks, the coating of batch I started to present optically ansotropic grains, as can be seen in Fig. 2(c). Increasing the annealing temperature to 900 °C resulted in complete crystallization of the coating, as shown in Fig. 2(d). The anisotropy of the grains confirms their crystalline nature, consistent with the GIXRD measurements.

In order to study the relation between surface topography and crystallization, we performed Atomic Force Microscopy (AFM) on as-deposited and annealed samples from batch I.

AFM topography maps are reported in Figs. 2(e–h), together with the corresponding phase maps in Figs. 2(i–l). Both the as-deposited sample and those annealed up to 800 °C show an almost atomically flat surface with few raised defects. When the coating was annealed at 850 °C, depressions appeared that were consistent with the size of crystalline grains observed under optical microscopy. These grains were also visible against the matrix in the phase map, which indicates a change in the interaction between the tip and the surface, due to a modification of the physical nature of the grains with respect to the amorphous matrix. The phase contrast visible in the different grains is presumably caused by the different orientations of the crystalline grains as seen with optical microscopy. This led us to conclude that the crystalline grains are denser than the amorphous matrix, resulting in local surface depressions. The same trend is observed in the completely crystallized sample annealed at 900 °C, which shows depressions at the center of each crystalline grain and raised boundaries between grains.

When examining thin films annealed at 500 °C or higher, regardless of composition, we observe round, bubble-like raised structures appearing on the coating surface (see Figure S.4). The structures are also visible in AFM topography and phase measurements, which we report in Figure S.5 for the partially crystallized sample from batch I annealed at 850 °C. EDX measurements show that the round structures have the same surface chemical composition as the surrounding matrix and grains. Together with their raised, domed shape, this led us to the

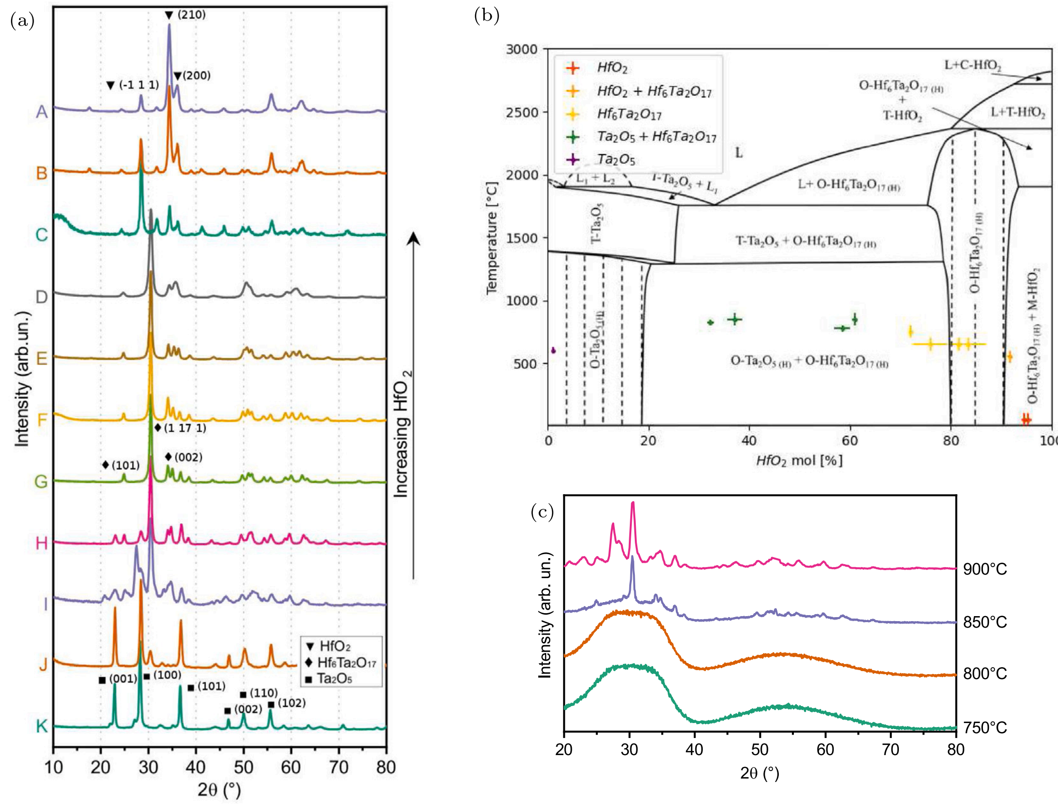

Fig. 1. (a) GIXRD diffractograms of samples annealed at 900 °C for 10 h. Three main crystalline phases have been identified: monoclinic HfO_2, orthorhombic $Hf_6Ta_2O_{17}$, and hexagonal Ta_2O_5 (respectively PDF 00-078-0049, PDF 00-044-0998, and PDF 00-019-1299). (b) Crystallization temperature for 10 h of annealing vs. hafnia molar concentration measured via EDX. The color of the data points represent the crystalline structure identified after the annealing. The background of the graph is the experimental HfO_2—Ta_2O_5 phase diagram by McCormack et al. [56] (reproduced with permission). (c) GIXRD of sample batch I.

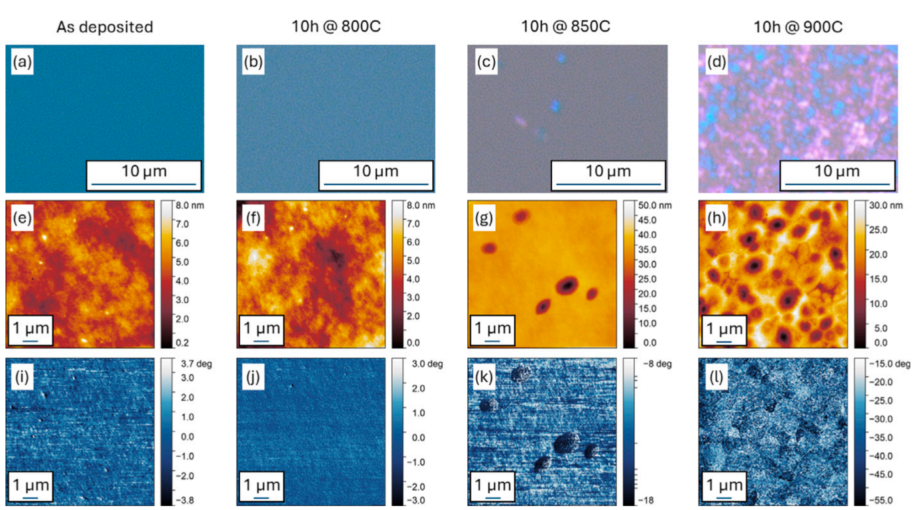

Fig. 2. (a–d) Optical microscopy, (e–h) AFM topography and (i–l) AFM phase of samples from batch I, as deposited (first column) and annealed for 10 h at 800 °C (second column), 850 °C (third column), 900 °C (fourth column).

conclusion that they are bubbles created by Ar gas desorption from the film during annealing. Blistering is a known issue in mirror coatings deposited via IBS, and recent models have linked it to several factors, ranging from Ar accumulation to substrate roughness [54,59].

Moreover, in the partially crystallized sample (annealed at 850 °C), we found that the domed structure is surrounded by grains, visible both in optical microscopy and AFM measurements (topography and phase maps). The observed higher density of crystalline grains at the edges of the bubbles is likely due to the edges providing a defect in the thin film structure which serves as preferred nucleation site.

3.3. Optical properties

For each as-deposited sample, we acquired Raman spectra and calculated their reduced form as follows [60]:

$$\mathcal{I}_R(\omega) = \frac{1}{n(\omega)} \frac{\omega}{(\omega_L - \omega)^4} \mathcal{I}_0(\omega), \tag{2}$$

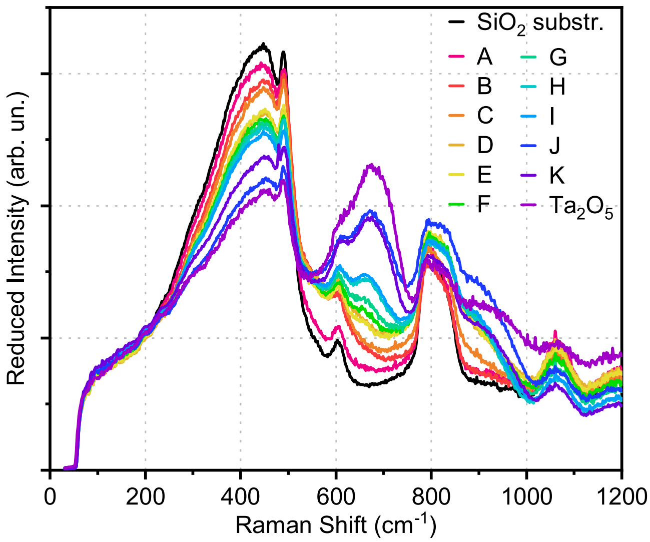

Fig. 3. Reduced Raman spectra of As Deposited samples from all batches listed in Table 1, calculated as in [60]. Spectra from the SiO_2 substrate and the Ta_2O_5 coating added for comparison.

where $\mathcal{I}_0(\omega)$ is the experimentally determined spectral intensity, ω_L is the incident laser frequency, and $n(\omega)$ is the following temperature-related boson factor:

$$n(\omega) = \left(\exp(\hbar\omega/k_B T) - 1\right)^{-1} \tag{3}$$

The reduced intensity $\mathcal{I}_R(\omega)$ can be represented as $\mathcal{I}_R(\omega) = C(\omega) \cdot \rho(\omega)$, where $C(\omega)$ is the coupling function and $\rho(\omega)$ is the vibrational density of states (VDOS) [60,61]. This procedure eliminates the peak asymmetry contributions due to phonon statistics and to the different resonance of vibrational peaks with the selected laser wavelength. Reduced Raman spectra for each composition are reported in Fig. 3, together with the background SiO_2 substrate signal and a Ta_2O_5 coating sample. Coatings with HfO_2 concentration > 90% (batches A to C) have a spectrum which is very close to that of the SiO_2 substrate. This similarity between the Raman signals of amorphous HfO_2 and SiO_2 is consistent with available literature and seems to be independent of the excitation wavelength [62,63].

At higher tantala concentrations, two broad peaks at approximately 670 cm^{-1} and 900 cm^{-1} increase in intensity, consistent with the literature for amorphous Ta_2O_5 [64,65]. Moreover, the SiO_2 broad peak at about 400 cm^{-1} decreases in intensity, which is consistent with dense Ta_2O_5 coatings masking the signal from the substrate.

The distribution of experimental data between the two extremes of pure amorphous Ta_2O_5 and SiO_2 closely matches the molar concentration of HfO_2 found in Table 1.

We used spectroscopic ellipsometry on amorphous samples to determine the refractive index as a function of the HfO_2 molar concentration. As noted earlier, Batches A and B, which showed crystallization as-deposited, were not optically homogeneous and were not considered for this analysis. Fig. 4 a,b shows the ellipsometry data Ψ and Δ measured on batch I. As the graphs show, the best fit and experimental data are perfectly matched. The same procedure was carried out for all amorphous as-deposited HfO_2:Ta_2O_5 mixes. Results in ellipsometry are typically obtained by means of a model-based analysis. It might happen that slightly different models (for example, two different dispersion formulae simulating the broad-band optical response of a coating layer) yield quite similar, yet not identical results. This uncertainty is represented by means of the error bars reported on the refractive index and energy gap. The refractive index and energy gap obtained from the data fitting are reported in Fig. 4 c, d.

Table 2
Measurements of CTN and optical absorption of multilayer HR samples with HfO_2:Ta_2O_5 layers. CTN values are given as a fraction of the Advanced LIGO value, $13.7 \cdot 10^{-18}$ m $Hz^{-1/2}$. (CTN amplitude values are given at 100 Hz).

Sample	Annealing T (°C)	CTN (fraction aLIGO)	Slope	Absorption (ppm)
aLIGO		1.00	0.45 ± 0.02	0.5
11618	as deposited	1.37 ± 0.02	0.42 ± 0.02	42.0 ± 16.8
11648	600	1.09 ± 0.02	0.41 ± 0.02	2.9 ± 1.2
11644	700	1.09 ± 0.02	0.41 ± 0.02	2.6 ± 1.0
11646	800	1.04 ± 0.02	0.42 ± 0.02	2.4 ± 1.0

For applications in GWD mirrors, it is often relevant to specify the refractive index of materials for mirrors at selected wavelengths. In Fig. 4(e) we report such values obtained with the Cody Lorentz optical model for sample I at four of the most commonly employed wavelengths, from the visible (532 nm) to the near infrared (2000 nm).

As seen in Fig. 4(c), the refractive index difference between pure Ta_2O_5 [50] and amorphous HfO_2:Ta_2O_5 thin films with the highest HfO_2 molar concentration (92%) is minimal, at less than 7% (i.e., excluding HfO_2:Ta_2O_5 films with crystalline inclusions in the as-deposited state). Therefore HfO_2:Ta_2O_5 mixtures are perfectly suitable for the role of HI material in GW mirrors.

3.4. Coating thermal noise

We measured the coating thermal noise (CTN) of four multilayer, HR coating samples made of HfO_2:Ta_2O_5 and SiO_2 thin layers and deposited in the same run (n. 11618, 11648, 11644 and 11646). Their HfO_2:Ta_2O_5 layers were deposited under the same conditions as sample I, but underwent annealing treatments at different temperatures. Chosen annealing temperatures were 600 °C, 700 °C and 800 °C, in order to remain below the crystallization temperature threshold. The target annealing temperature was maintained for 10 h, as for the monolayer samples.

As an example, the amplitude spectral density of the total measured noise of the HfO_2:Ta_2O_5 sample annealed to 800 °C is shown in red in Fig. 5, together with a reference CTN measurement of an Advanced LIGO (aLIGO) end test mass witness sample (dashed green line). By fitting a power law to the spectra between ∼ 40 Hz and ∼ 2 kHz (dashed blue curve in Fig. 5), we were able to determine the frequency dependence of the observed CTN,

$$\mathrm{CTN}(f) = \mathrm{CTN} \times \left(\frac{100\mathrm{Hz}}{f}\right)^{\mathrm{slope}} \tag{4}$$

The fitted values of the slope and the CTN amplitudes at 100 Hz, expressed as a ratio to the currently available aLIGO CTN ($13.7 \cdot 10^{-18}$ m $Hz^{-1/2}$), as sensed by 02+20 Hermite Gaussian modes with a 50 μm beam spot size, are shown in Table 2. The as-deposited mirror (n. 11618) had the highest CTN, a factor of 1.37 larger than that of the Advanced LIGO coatings. As the annealing temperature increased, the CTN decreased, as expected from available literature [4]. Annealing at 600 °C reduced the CTN by 20%, reaching 1.09 times that of the aLIGO coatings. The mirror annealed to 800 °C (n. 11646) had the lowest CTN, only 1.04 times higher than that of the aLIGO coatings.

We also used our CTN setup, as described in paragraph 2.2.7, to measure the optical absorption at 1064 nm, the wavelength of light relevant for current gravitational-wave detectors [14,52,53]. By comparison with previous studies, we expect optical absorption to decrease upon annealing [4]. The unannealed mirror (n. 11618) had 42 parts per million (ppm) absorption, more than 80 times the value measured for aLIGO mirrors. Annealing decreased the absorption by an order of magnitude. Absorption decreased further with increasing annealing temperatures until arriving at a 2.4 ppm for the mirror annealed at

Optical Materials 163 (2025) 116901

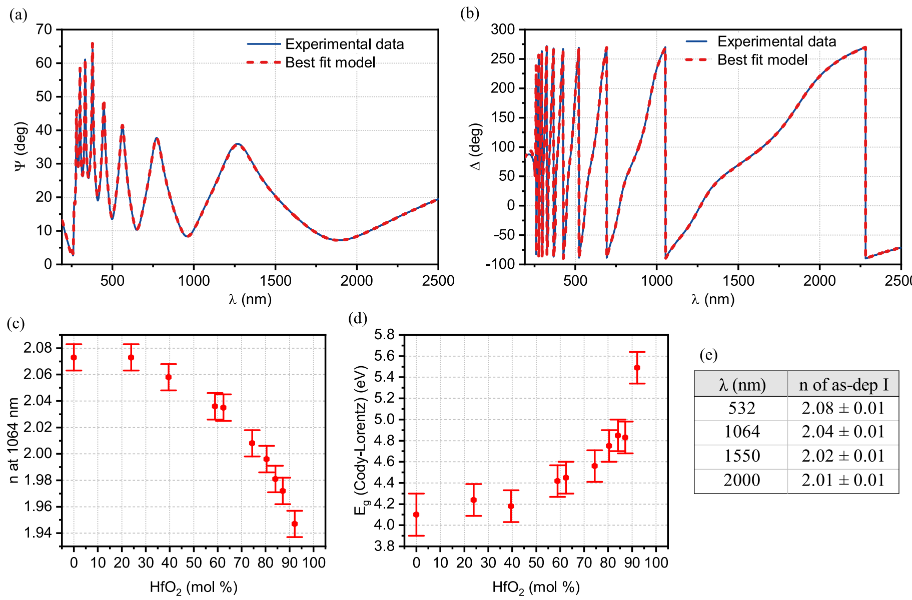

λ (nm)	n of as-dep I
532	2.08 ± 0.01
1064	2.04 ± 0.01
1550	2.02 ± 0.01
2000	2.01 ± 0.01

Fig. 4. (a) *Ψ* and (b) *Δ* spectra for sample I at the angle of incidence of 70°. Experimental data (continuous lines) and best-fit model (dashed lines) are reported in the same plot for comparison. (c) Refractive index at 1064 nm and (d) energy gap obtained from the SE data modeling. Pure Ta coatings data, gathered with the same experimental protocol, from [50]. (e) Refractive index *n* of as deposited sample from batch I as a function of the wavelength.

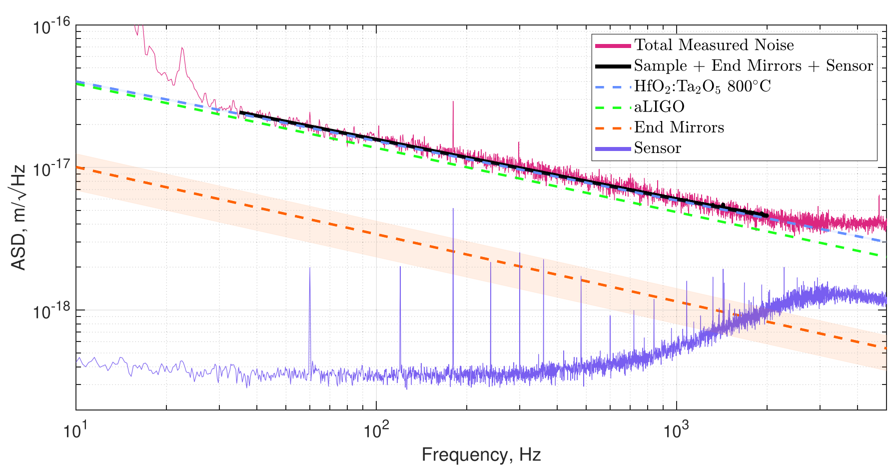

Fig. 5. The total measured noise of the HfO_2:Ta_2O_5 sample annealed to 800 °C, given as an amplitude spectral density (ASD), is shown in red. The dashed blue "HfO_2:Ta_2O_5 800 °C" curve is the fitted CTN of the sample mirror. The orange "End Mirrors" curve is the combined CTN of the input and output cavity mirrors, previously measured and scaled appropriately. The shaded orange region represents one standard deviation uncertainty on the CTN of the end mirrors. The purple sensor curve is a combination of the noise from electronics and the shot noise on the photodetectors. The black curve through the total measured noise is the combined fit of the sample CTN, the end mirrors CTN, and the sensor noise. The aLIGO curve is the CTN of a previously measured aLIGO end test mass witness sample and is provided for reference.

800 °C (n. 11646), only five times the value measured for the aLIGO mirrors.

Consistent with our expectations, we observed a reduction in both CTN and optical absorption upon annealing. It is worth noting that, thanks to the high temperature annealing made possible by the improved thermal stability of our HfO_2:Ta_2O_5 coatings with optimized composition (about 60% HfO_2 molar content, sample I) it was possible to obtain results comparable with the highly-optimized TiO_2:Ta_2O_5 coatings used in LIGO and Virgo. This is a remarkable result since both the deposition process and the stack design in the multilayer mirror are still to be optimized, leaving room for considerable improvement. Hence HfO_2:Ta_2O_5 with enhanced thermal stability is a promising HI candidate material for GW mirrors, warranting future investigation and optimization.

4. Discussion and conclusions

In this work, we investigated the thermal noise properties of HfO:Ta_2O_5 mixes with high thermal stability and annealed at high temperatures. A set of samples with different compositions were studied to determine which one would best withstand a strong annealing at high temperature for 10 h remaining in the amorphous state. The best mix (about 60% mol. HfO_2) could be annealed at temperatures as high as 800 °C without crystallizing. This material has been employed as a HI layer in a Bragg mirror made of a SiO_2/HfO_2:Ta_2O_5 quarter-wave stack which, even without optimization, displayed mechanical performances comparable to those of the best LIGO-Virgo mirrors.

Most crucially, we demonstrated in this work the importance of considering the *thermal stability* of the HI layers. The driving idea motivating our whole study was that by enhancing thermal stability, we could perform annealing in (high temperature) conditions enabling us to achieve a higher degree of structural relaxation without losing the amorphous character of the material. The drastic decrease of coating thermal noise we observe after annealing our HfO_2:Ta_2O_5 sample at 800 °C is a direct and successful experimental test of this idea. This also suggests that, in addition to material formulation through the deposition process, future optimizations could involve developing tailored annealing protocols to more effectively leverage the thermal stability range of a given mixture, obviously taking into account other parameters contributing to the overall CTN of the whole stack such as e.g. the refractive index of the layer or its optical absorption.

This achievement, of course, underlines the importance of material analysis in the field of GW detection, as optimizing the mirror coating materials is going to be very important to reach the sensitivity goals of advanced second and third generation GW detectors.

CRediT authorship contribution statement

Valeria Milotti: Writing – review & editing, Writing – original draft, Visualization, Software, Methodology, Investigation, Formal analysis, Data curation. **Giulio Favaro:** Writing – review & editing, Visualization, Validation, Software, Methodology, Investigation, Formal analysis, Data curation, Conceptualization. **Massimo Granata:** Writing – review & editing, Resources, Methodology, Conceptualization. **Danièle Forest:** Resources, Funding acquisition. **Christophe Michel:** Resources, Funding acquisition. **Julien Teillon:** Resources. **Nicole Busdon:** Validation, Investigation. **Marco Bazzan:** Writing – review & editing, Validation, Supervision, Resources, Project administration, Funding acquisition, Conceptualization. **Hanna Skliarova:** Writing – review & editing, Validation. **Giacomo Ciani:** Writing – review & editing, Validation, Supervision, Project administration. **Carlo Scian:** Visualization, Investigation, Formal analysis. **Livia Conti:** Writing – review & editing, Validation, Supervision, Methodology. **Shima Samandari:** Investigation, Formal analysis, Data curation. **Valentina Venturino:** Investigation, Formal analysis, Data curation. **Michele Magnozzi:** Writing – review & editing, Visualization, Supervision, Methodology, Investigation, Formal analysis, Data curation. **Maurizio Canepa:** Writing – review & editing, Supervision, Project administration, Funding acquisition. **Nicholas Demos:** Writing – review & editing, Visualization, Methodology, Investigation, Formal analysis. **Slawomir Gras:** Methodology, Investigation. **Matthew Evans:** Methodology, Investigation. **Valérie Martinez:** Methodology, Investigation. **Gianpietro Cagnoli:** Supervision, Project administration, Funding acquisition. **Nikita S. Shcheblanov:** Conceptualization. **Anaël Lemaître:** Writing – review & editing, Validation, Supervision, Methodology, Funding acquisition, Conceptualization.

Declaration of competing interest

The authors declare that they have no known competing financial interests or personal relationships that could have appeared to influence the work reported in this paper.

Acknowledgments

VM, NB and HS gratefully acknowledge the support of the Italian MUR through the national project PNRR - ETIC. NB gratefully acknowledges also the support of the Italian MUR Departments of Excellence grant 2023–2027 "Quantum Frontiers". This work benefited from the support of the French National Research Agency (ANR) via the ViSIONs project (grant n. ANR-18-CE08-0023-03) and the Programme d'investissements d'avenir framework (grant n. ANR-11-LABX-0022-01). CTN data analysis and figure generation was carried out using MATLAB software provided by The MathWorks, Inc. LIGO was constructed by the California Institute of Technology and Massachusetts Institute of Technology with funding from the National Science Foundation and operates under cooperative agreement PHY-1764464. Virgo is funded through the European Gravitational Observatory (EGO) by the French Centre National de Recherche Scientifique (CNRS), the Italian Istituto Nazionale di Fisica Nucleare (INFN), and the Dutch Nikhef, with contributions from institutions in Belgium, Germany, Greece, Hungary, Ireland, Japan, Monaco, Poland, Portugal, and Spain

Appendix A. Supplementary data

Supplementary material related to this article can be found online at https://doi.org/10.1016/j.optmat.2025.116901.

Data availability

Data will be made available on request.

References

[1] The LIGO Scientific Collaboration, et al., Advanced LIGO, Cl. Quantum Grav. 32 (7) (2015) 074001, http://dx.doi.org/10.1088/0264-9381/32/7/074001.

[2] D.R.M. Crooks, P. Sneddon, G. Cagnoli, J. Hough, S. Rowan, M.M. Fejer, E. Gustafson, R. Route, N. Nakagawa, D. Coyne, G.M. Harry, A.M. Gretarsson, Excess mechanical loss associated with dielectric mirror coatings on test masses in interferometric gravitational wave detectors, Cl. Quantum Grav. 19 (5) (2002) 883–896, http://dx.doi.org/10.1088/0264-9381/19/5/304.

[3] F. Acernese, M. Agathos, K. Agatsuma, D. Aisa, N. Allemandou, A. Allocca, J. Amarni, P. Astone, G. Balestri, G. Ballardin, et al., Advanced Virgo: a second-generation interferometric gravitational wave detector, Cl. Quantum Grav. 32 (2) (2014) 024001, http://dx.doi.org/10.1088/0264-9381/32/2/024001.

[4] M. Granata, A. Amato, L. Balzarini, M. Canepa, J. Degallaix, D. Forest, V. Dolique, L. Mereni, C. Michel, L. Pinard, B. Sassolas, J. Teillon, G. Cagnoli, Amorphous optical coatings of present gravitational-wave interferometers, Cl. Quantum Grav. 37 (9) (2020) 095004, http://dx.doi.org/10.1088/1361-6382/ab77e9.

[5] J. Degallaix, C. Michel, B. Sassolas, A. Allocca, G. Cagnoli, L. Balzarini, V. Dolique, R. Flaminio, D. Forest, M. Granata, B. Lagrange, N. Straniero, J. Teillon, L. Pinard, Large and extremely low loss: the unique challenges of gravitational wave mirrors, J. Opt. Soc. Amer. A 36 (2019) C85–C94, http://dx.doi.org/10.1364/JOSAA.36.000C85, URL https://opg.optica.org/josaa/abstract.cfm?URI=josaa-36-11-C85.

[6] L. Pinard, C. Michel, B. Sassolas, L. Balzarini, J. Degallaix, V. Dolique, R. Flaminio, D. Forest, M. Granata, B. Lagrange, N. Straniero, J. Teillon, G. Cagnoli, Mirrors used in the LIGO interferometers for first detection of gravitational waves, Appl. Opt. 56 (2017) C11–C15, http://dx.doi.org/10.1364/AO.56.000C11, URL https://opg.optica.org/ao/abstract.cfm?URI=ao-56-4-C11.

[7] G.M. Harry, M.R. Abernathy, A.E. Becerra-Toledo, H. Armandula, E. Black, K. Dooley, M. Eichenfield, C. Nwabugwu, A. Villar, D.R.M. Crooks, G. Cagnoli, J. Hough, C.R. How, I. MacLaren, P. Murray, S. Reid, S. Rowan, P.H. Sneddon, M.M. Fejer, R. Route, S.D. Penn, P. Ganau, J.-M. Mackowski, C. Michel, L. Pinard, A. Remillieux, Titania-doped tantala/silica coatings for gravitational-wave detection, Cl. Quantum Grav. 24 (2) (2006) 405–415, http://dx.doi.org/10.1088/0264-9381/24/2/008.

[8] G.M. Harry, H. Armandula, E. Black, D.R.M. Crooks, G. Cagnoli, J. Hough, P. Murray, S. Reid, S. Rowan, P. Sneddon, M.M. Fejer, R. Route, S.D. Penn, Thermal noise from optical coatings in gravitational wave detectors, Appl. Opt. 45 (7) (2006) 1569, http://dx.doi.org/10.1364/ao.45.001569.

[9] A.E. Villar, E.D. Black, R. DeSalvo, K.G. Libbrecht, C. Michel, N. Morgado, L. Pinard, I.M. Pinto, V. Pierro, V. Galdi, M. Principe, I. Taurasi, Measurement of thermal noise in multilayer coatings with optimized layer thickness, Phys. Rev. D 81 (12) (2010) 122001, http://dx.doi.org/10.1103/physrevd.81.122001.

[10] The Einstein Telescope Steering Committee, Einstein Telescope Design Report Update, Technical Note ET-0007C-20, 2020, Available at https://apps.et-gw.eu/tds/ql/?c=15418.

[11] E.D. Hall, Cosmic Explorer: A next-generation ground-based gravitational-wave observatory, Galaxies 10 (2022) http://dx.doi.org/10.3390/galaxies10040090, URL https://www.mdpi.com/2075-4434/10/4/90.

[12] M. Granata, A. Amato, G. Cagnoli, M. Coulon, J. Degallaix, D. Forest, L. Mereni, C. Michel, L. Pinard, B. Sassolas, J. Teillon, Progress in the measurement and reduction of thermal noise in optical coatings for gravitational-wave detectors, Appl. Opt. 59 (5) (2020) A229, http://dx.doi.org/10.1364/ao.377293.

[13] G. Vajente, L. Yang, A. Davenport, M. Fazio, A. Ananyeva, L. Zhang, G. Billingsley, K. Prasai, A. Markosyan, R. Bassiri, et al., Low mechanical loss TiO_2:GeO_2 coatings for reduced thermal noise in gravitational wave interferometers, Phys. Rev. Lett. 127 (7) (2021) 071101.

[14] G.I. McGhee, V. Spagnuolo, N. Demos, S.C. Tait, P.G. Murray, M. Chicoine, P. Dabadie, S. Gras, J. Hough, G.A. Iandolo, et al., Titania mixed with silica: A low thermal-noise coating material for gravitational-wave detectors, Phys. Rev. Lett. 131 (17) (2023) 171401, http://dx.doi.org/10.1103/PhysRevLett.131.171401.

[15] B.P. Abbott, R. Abbott, T.D. Abbott, M.R. Abernathy, F. Acernese, K. Ackley, C. Adams, T. Adams, P. Addesso, R.X. Adhikari, et al., GW150914: The Advanced LIGO detectors in the era of first discoveries, Phys. Rev. Lett. 116 (13) (2016) 131103, http://dx.doi.org/10.1103/physrevlett.116.131103.

[16] S. Hild, M. Abernathy, F. Acernese, P. Amaro-Seoane, N. Andersson, K. Arun, F. Barone, B. Barr, M. Barsuglia, M. Beker, et al., Sensitivity studies for third-generation gravitational wave observatories, Cl. Quantum Grav. 28 (9) (2011) 094013, http://dx.doi.org/10.1088/0264-9381/28/9/094013.

[17] W.A. Phillips, Two-level states in glasses, Rep. Progr. Phys. 50 (12) (1987) 1657–1708, http://dx.doi.org/10.1088/0034-4885/50/12/003.

[18] J. Burnett, L. Faoro, I. Wisby, V.L. Gurtovoi, A.V. Chernykh, G.M. Mikhailov, V.A. Tulin, R. Shaikhaidarov, V. Antonov, P.J. Meeson, A.Y. Tzalenchuk, T. Lindström, Evidence for interacting two-level systems from the 1/f noise of a superconducting resonator, Nat. Commun. 5 (1) (2014) http://dx.doi.org/10.1038/ncomms5119.

[19] R. Hamdan, J.P. Trinastic, H.P. Cheng, Molecular dynamics study of the mechanical loss in amorphous pure and doped silica, J. Chem. Phys. 141 (5) (2014) http://dx.doi.org/10.1063/1.4890958.

[20] J.P. Trinastic, R. Hamdan, C. Billman, H.-P. Cheng, Molecular dynamics modeling of mechanical loss in amorphous tantala and titania-doped tantala, Phys. Rev. B 93 (1) (2016) 014105, http://dx.doi.org/10.1103/physrevb.93.014105.

[21] C.R. Billman, J.P. Trinastic, D.J. Davis, R. Hamdan, H.-P. Cheng, Origin of the second peak in the mechanical loss function of amorphous silica, Phys. Rev. B 95 (1) (2017) 014109, http://dx.doi.org/10.1103/physrevb.95.014109.

[22] L.-C. Kuo, H.-W. Pan, C.-L. Chang, S. Chao, Low cryogenic mechanical loss composite silica thin film for low thermal noise dielectric mirror coatings, Opt. Lett. 44 (2) (2019) 247, http://dx.doi.org/10.1364/ol.44.000247.

[23] S. Singh, M.D. Ediger, J.J. de Pablo, Ultrastable glasses from in silico vapour deposition, Nat. Mater. 12 (2) (2013) 139–144, http://dx.doi.org/10.1038/nmat3521, URL DOI: 10.1038/nmat3521.

[24] T. Perez-Castaneda, C. Rodriguez-Tinoco, J. Rodriguez-Viejo, M.A. Ramos, Suppression of tunneling two-level systems in ultrastable glasses of indomethacin, Proc. Natl. Acad. Sci. USA 111 (31) (2014) 11275–11280, http://dx.doi.org/10.1073/pnas.1405545111.

[25] Y. Zhao, B. Shang, B. Zhang, X. Tong, H. Ke, H. Bai, W.H. Wang, Ultrastable metallic glass by room temperature aging, Sci. Adv. 8 (33) (2022) eabn3623, http://dx.doi.org/10.1126/sciadv.abn3623, http://arxiv.org/abs/https://www.science.org/doi/pdf/10.1126/sciadv.abn3623 URL https://www.science.org/doi/abs/10.1126/sciadv.abn3623.

[26] J.Q. Wang, N. Chen, P. Liu, Z. Wang, D.V. Louzguine-Luzgin, M.W. Chen, J.H. Perepezko, The ultrastable kinetic behavior of an Au-based nanoglass, Acta Mater. 79 (2014) 30–36, http://dx.doi.org/10.1016/j.actamat.2014.07.015.

[27] M.A. Fazio, L. Yang, C.S. Menoni, Prediction of crystallized phases of amorphous Ta_2O_5-based mixed oxide thin films using a density functional theory database, APL Mater. 9 (3) (2021) 031106, http://dx.doi.org/10.1063/5.0035573.

[28] A. Sezgin, R. Čtvrtlík, L. Václavek, J. Tomáštík, L. Nožka, E. Menşur, S. Türküz, Optical, structural and mechanical properties of TiO_2 and TiO_2-ZrO_2 thin films deposited on glass using magnetron sputtering, Mater. Today Commun. 35 (2023) 106334, http://dx.doi.org/10.1016/j.mtcomm.2023.106334, URL https://www.sciencedirect.com/science/article/pii/S2352492823010255.

[29] G. Favaro, V. Milotti, D. Alonso Diaz Riega, N. Busdon, M. Bazzan, M. Granata, D. Hofman, C. Michel, L. Pinard, L. Conti, S. Capaccioli, N.S. Shcheblanov, A. Lemaître, V. Martinez, G. Cagnoli, F. Piergiovanni, F. Fabrizi, M.G. Pelizzo, A.J. Corso, Reduction of mechanical losses in ion-beam sputtered tantalum oxide thin films via partial crystallization, Cl. Quantum Grav. 41 (10) (2024) 105009, http://dx.doi.org/10.1088/1361-6382/ad3c8a.

[30] W.H. Wang, C. Dong, C.H. Shek, Bulk metallic glasses, Mater. Sci. Eng. R- Rep. 44 (2–3) (2004) 45–89, http://dx.doi.org/10.1016/j.mser.2004.03.001.

[31] C. Stabler, F. Celarie, T. Rouxel, R. Limbach, L. Wondraczek, R. Riedel, E. Ionescu, Effect of composition and high-temperature annealing on the local deformation behavior of silicon oxycarbides, J. Eur. Ceram. Soc. 39 (7) (2019) 2287–2296, http://dx.doi.org/10.1016/j.jeurceramsoc.2019.02.024, URL https://www.sciencedirect.com/science/article/pii/S0955221919301049.

[32] P. Mezeix, T. To, P. Houizot, F. Célarié, T. Rouxel, Crystallization and mechanical properties of a barium titanosilicate glass, J. Mater. Sci. 59 (11) (2024) 4620–4635, http://dx.doi.org/10.1007/s10853-024-09518-3.

[33] A. Inoue, Stabilization of metallic supercooled liquid and bulk amorphous alloys, Acta Mater. 48 (1) (2000) 279–306, http://dx.doi.org/10.1016/S1359-6454(99)00300-6.

[34] W.H. Wang, Roles of minor additions in formation and properties of bulk metallic glasses, Prog. Mater. Sci. 52 (4) (2007) 540–596, http://dx.doi.org/10.1016/j.pmatsci.2006.07.003.

[35] M.A. Fazio, L. Yang, C.S. Menoni, Prediction of crystallized phases of amorphous Ta_2O_5-based mixed oxide thin films using a density functional theory database, APL Mater. 9 (3) (2021) http://dx.doi.org/10.1063/5.0035573.

[36] M.A. Fazio, G. Vajente, L. Yang, A. Ananyeva, C.S. Menoni, Comprehensive study of amorphous metal oxide and Ta_2O_5-based mixed oxide coatings for gravitational-wave detectors, Phys. Rev. D 105 (10) (2022) 102008, http://dx.doi.org/10.1103/physrevd.105.102008.

[37] C. Zhao, Z.M. Rittersma, J.G.M. Van Berkum, J.H.M. Snijders, A. Hendriks, P. Breimer, P. Graat, J.W. Maes, H. De Witter, V.V. Afanas'ev, E. Tois, M. Tuominen, M. Caymax, S. De Gendt, M. Heyns, Properties of HfTaxOy high-K layers deposited by ALCVD, ECS Meet. Abstr. MA2005-01 (14) (2006) 622, http://dx.doi.org/10.1149/ma2005-01/14/622.

[38] F. Beauville, D. Buskulic, R. Flaminio, F. Marion, A. Masserot, L. Massonnet, B. Mours, F. Moreau, J. Ramonet, E. Tournefier, et al., The VIRGO large mirrors: a challenge for low loss coatings, Cl. Quantum Grav. 21 (2004) S935, http://dx.doi.org/10.1088/0264-9381/21/5/083.

[39] A. Altomare, C. Cuocci, C. Giacovazzo, A. Moliterni, R. Rizzi, QUALX: a computer program for qualitative analysis using powder diffraction data, J. Appl. Crystallogr. 41 (4) (2008) 815–817, http://dx.doi.org/10.1107/s0021889808016956.

[40] A. Altomare, N. Corriero, C. Cuocci, A. Falcicchio, A. Moliterni, R. Rizzi, QUALX2.0: a qualitative phase analysis software using the freely available database POW_COD, J. Appl. Crystallogr. 48 (2) (2015) 598–603, http://dx.doi.org/10.1107/s1600576715002319.

[41] R.T. Downs, M. Hall-Wallace, The American mineralogist crystal structure database, Am. Mineral. 88 (2003) 247–250.

[42] S. Gražulis, D. Chateigner, R.T. Downs, A.F.T. Yokochi, M. Quirós, L. Lutterotti, E. Manakova, J. Butkus, P. Moeck, A. Le Bail, Crystallography Open Database – an open-access collection of crystal structures, J. Appl. Crystallogr. 42 (4) (2009) 726–729, http://dx.doi.org/10.1107/S0021889809016690.

[43] S. Gražulis, A. Daškevič, A. Merkys, D. Chateigner, L. Lutterotti, M. Quirós, N.R. Serebryanaya, P. Moeck, R.T. Downs, A. Le Bail, Crystallography open database (COD): an open-access collection of crystal structures and platform for world-wide collaboration, Nucleic Acids Res. 40 (D1) (2012) D420–D427, http://dx.doi.org/10.1093/nar/gkr900, http://arxiv.org/abs/https://nar.oxfordjournals.org/content/40/D1/D420.full.pdf+html URL https://academic.oup.com/nar/article/40/D1/D420/2903497.

[44] A. Merkys, A. Vaitkus, J. Butkus, M. Okulič-Kazarinas, V. Kairys, S. Gražulis, *COD::CIF::Parser*: an error-correcting CIF parser for the Perl language, J. Appl. Crystallogr. 49 (1) (2016) http://dx.doi.org/10.1107/S1600576715022396.

[45] M. Quirós, S. Gražulis, S. Girdzijauskaitė, A. Merkys, A. Vaitkus, Using SMILES strings for the description of chemical connectivity in the Crystallography Open Database, J. Cheminf. 10 (1) (2018) http://dx.doi.org/10.1186/s13321-018-0279-6.

[46] A. Vaitkus, A. Merkys, S. Gražulis, Validation of the crystallography open database using the crystallographic information framework, J. Appl. Crystallogr. 54 (2) (2021) 661–672, http://dx.doi.org/10.1107/S1600576720016532.

[47] A. Merkys, A. Vaitkus, A. Grybauskas, A. Konovalovas, M. Quirós, S. Gražulis, Graph isomorphism-based algorithm for cross-checking chemical and crystallographic descriptions, J. Cheminf. 15 (1) (2023) http://dx.doi.org/10.1186/s13321-023-00692-1.

[48] A. Vaitkus, A. Merkys, T. Sander, M. Quirós, P.A. Thiessen, E.E. Bolton, S. Gražulis, A workflow for deriving chemical entities from crystallographic data and its application to the Crystallography Open Database, J. Cheminf. 15 (1) (2023) http://dx.doi.org/10.1186/s13321-023-00780-2, URL DOI: 10.1186/s13321-023-00780-2.

[49] H. Fujiwara, Spectroscopic Ellipsometry, John Wiley & Sons, Chichester, 2007.

[50] A. Amato, M. Magnozzi, N. Shcheblanov, A. Lemaître, G. Cagnoli, M. Granata, C. Michel, G. Gemme, L. Pinard, M. Canepa, Enhancing titania-tantala amorphous materials as high-index layers in bragg reflectors of gravitational-wave detectors, AC Appl Opt Mater. 1 (1) (2023) 395–402, http://dx.doi.org/10.1021/acsaom.2c00077.

[51] JA Woollam Co., Inc., WVASE manual. Guide to using WVASE32, 2010.

[52] S. Gras, M. Evans, Direct measurement of coating thermal noise in optical resonators, Phys. Rev. D 98 (2018) 122001, http://dx.doi.org/10.1103/PhysRevD.98.122001, URL https://link.aps.org/doi/10.1103/PhysRevD.98.122001.

[53] S. Gras, H. Yu, W. Yam, D. Martynov, M. Evans, Audio-band coating thermal noise measurement for Advanced LIGO with a multimode optical resonator, Phys. Rev. D 95 (2017) 022001, http://dx.doi.org/10.1103/PhysRevD.95.022001, URL https://link.aps.org/doi/10.1103/PhysRevD.95.022001.

[54] A. Amato, G. Cagnoli, M. Granata, B. Sassolas, J. Degallaix, D. Forest, C. Michel, L. Pinard, N. Demos, S. Gras, M. Evans, A. Di Michele, M. Canepa, Optical and mechanical properties of ion-beam-sputtered Nb_2O_5 and TiO_2—Nb_2O_5 thin films for gravitational-wave interferometers and an improved measurement of coating thermal noise in Advanced LIGO, Phys. Rev. D 103 (7) (2021) 072001, http://dx.doi.org/10.1103/physrevd.103.072001.

[55] A. Paolone, E. Placidi, E. Stellino, M.G. Betti, E. Majorana, C. Mariani, A. Nucara, O. Palumbo, P. Postorino, M. Sbroscia, F. Trequattrini, M. Granata, D. Hofman, C. Michel, L. Pinard, A. Lemaitre, N. Shcheblanov, G. Cagnoli, F. Ricci, Argon and other defects in amorphous SiO_2 coatings for gravitational-wave detectors, Coat. J. 12 (7) (2022) 1001, http://dx.doi.org/10.3390/coatings12071001.

[56] S. McCormack, K.-P. Tseng, J. Weber, D. Kapush, S. Ushakov, A. Navrotsky, In-situ determination of the HfO_2—Ta_2O_5-temperature phase diagram up to 3000°C, J. Am. Ceram. Soc. 102 (2019) http://dx.doi.org/10.1111/jace.16271.

[57] S.J. McCormack, R.J. Weber, W.M. Kriven, In-situ investigation of $Hf_6Ta_2O_{17}$ anisotropic thermal expansion and topotactic, peritectic transformation, Acta Mater. 161 (2018) 127–137, http://dx.doi.org/10.1016/j.actamat.2018.08.029.

[58] S.J. McCormack, K.-P. Tseng, R.J.K. Weber, D. Kapush, S.V. Ushakov, A. Navrotsky, W.M. Kriven, In-situ determination of the HfO_2–Ta_2O_5-temperature phase diagram up to 3000° C, J. Am. Ceram. Soc. 102 (8) (2019) 4848–4861, http://dx.doi.org/10.1111/jace.16271.

[59] É. Lalande, A. Davenport, L. Marchand, A. Markosyan, D. Martinez, A. Paolone, M. Rezac, M. Bazzan, M. Chicoine, J.L. Colaux, M. Coulon, M.M. Fejer, A.W. Lussier, E. Majorana, L. Martinu, C. Menoni, C. Michel, F. Ricci, F. Schiettekatte, N. Shcheblanov, J.R. Smith, J. Teillon, G. Terwagne, G. Vajente, Ar transport and blister growth kinetics in titania-doped germania-based optical coatings, Cl. Quantum Grav. 41 (11) (2024) 115013, http://dx.doi.org/10.1088/1361-6382/ad3ffb.

[60] P. Umari, A. Pasquarello, First-principles analysis of the Raman spectrum of vitreous silica: comparison with the vibrational density of states, J. Condens. Matter Phys. 15 (16) (2003) S1547–S1552, http://dx.doi.org/10.1088/0953-8984/15/16/304.

[61] M.H. Brooker, O.F. Nielsen, E. Praestgaard, Assessment of correction procedures for reduction of Raman spectra, J. Raman Spectrosc. 19 (2) (1988) 71–78, http://dx.doi.org/10.1002/jrs.1250190202.

[62] G. Belo, F. Nakagomi, A. Minko, S. da Silva, P. Morais, D. Buchanan, Phase transition in sputtered HfO_2 thin films: A qualitative Raman study, Appl. Surf. Sci. 261 (2012) 727–729, http://dx.doi.org/10.1016/j.apsusc.2012.08.088.

[63] P. Borowicz, A. Taube, W. Rzodkiewicz, M. Latek, S. Gierałtowska, Raman spectra of high-κ dielectric layers investigated with micro-Raman spectroscopy comparison with silicon dioxide, in: D. Acevedo, A.G. Magalhães, A. Tonkikh (Eds.), Sci. World J. 2013 (1) (2013) http://dx.doi.org/10.1155/2013/208081.

[64] C. Joseph, P. Bourson, M.D. Fontana, Amorphous to crystalline transformation in Ta_2O_5 studied by Raman spectroscopy, J. Raman Spectrosc. 43 (8) (2012) 1146–1150, http://dx.doi.org/10.1002/jrs.3142.

[65] A. Amato, G. Cagnoli, M. Canepa, E. Coillet, J. Degallaix, V. Dolique, D. Forest, M. Granata, V. Martinez, C. Michel, L. Pinard, B. Sassolas, J. Teillon, High-reflection coatings for gravitational-wave detectors: State of the art and future developments, J. Phys.: Conf. Ser. 957 (2018) 012006, http://dx.doi.org/10.1088/1742-6596/957/1/012006.